Higgs boson signal at complete tree level in the SM extension by dimension-six operators

E. Boos,[1] V. Bunichev,[1] M. Dubinin,[1] and Y. Kurihara[2]

[1]*Skobeltsyn Institute of Nuclear Physics, Moscow State University, 119991 Moscow, Russia*
[2]*High Energy Accelerators Research Organization (KEK), Tsukuba, Ibaraki-ken 305-0801, Japan*

(Received 31 October 2013; published 4 February 2014)

Deviations from the standard Higgs sector generated by some new (nonstandard) physics at an energy scale Λ could be described by effective $\mathrm{SU}(3)_c \times \mathrm{SU}(2)_L \times \mathrm{U}(1)$ invariant nonrenormalizable Lagrangian terms of dimension six. The set of dimension-six operators involving the Higgs field is chosen in such a way that the form of the gauge boson kinetic terms remains untouched, preserving all high-precision electroweak constraints. A systematic study of effects in various Higgs boson production channels ($\gamma\gamma$, ZZ, WW, $b\bar{b}$, $\tau\bar{\tau}$) caused by effective operators is carried out beyond the production × decay approximation (or infinitely small width approximation). Statistical methods are used to establish the consistency of the standard Higgs sector with the available LHC data. A global fit in the two-parametric anomalous coupling space indicating possible deviations from the standard Higgs-fermion and Higgs-gauge boson couplings is performed, using post-Moriond 2012 data and more precise LC2013 data. We find that the standard Higgs sector is consistent with the current CMS and ATLAS experimental results both in the infinitely small width approximation and the calculation with complete gauge-invariant sets of diagrams. However, a visible difference between the exclusion contours is found for some combinations of production and decay channels, although it is minor for the global fits for all possible channels. Updates of the signal strength and the signal strength error reported at LC2013 result in significant improvements of the allowed regions in the anomalous coupling space, which are also recalculated at complete tree level.

DOI: 10.1103/PhysRevD.89.035001 PACS numbers: 14.80.Bn, 12.60.Fr, 11.10.Ef, 14.80.Ec

I. INTRODUCTION

The discovery of a Higgs-like signal at the LHC [1] provides the possibility of completing the Standard Model (SM), which is considered an effective theory at the energy scale $v = 246$ GeV rather than a self-contained field theory model. Physical observables up to energies of the order of the "new physics" scale Λ are described by an effective Lagrangian which can be written as an expansion in inverse powers of Λ. It is usually assumed that the electroweak symmetry-breaking scale v is disconnected from the scale of new physics Λ, so the effective Lagrangian terms are invariant with respect to the gauge group $\mathrm{SU}(3)_c \times \mathrm{SU}(2)_L \times \mathrm{U}(1)_Y$. Effective operators—first introduced in connection with a hypothetical baryon number violation and the four-fermion contact interactions [2]—have been used [3] to consider flavor-changing neutral currents, extended technicolor models, composite models, and other beyond the Standard Model extensions. In the following we use the results of a systematic study [4] where sector-by-sector extensions of the SM by dimension-five and dimension-six effective operators were performed. An improved classification of anomalous terms, where some redundant dimension-six operators were excluded, can be found in Ref. [5]. An equivalent basis, which isolates in a more convenient manner the operators essential for the decays $H \to \gamma\gamma$, γZ has been elaborated in Ref. [6] including higher-order corrections. Insofar as the effective Lagrangian terms include classical fields, the equations of motion can be used for simplifications[1] in both the scalar-fermion and scalar-gauge boson sectors, giving the following set of dimension-six operators:

(i) *Scalar-gauge boson sector*

$$
\begin{aligned}
O_{\Phi G} &= \frac{1}{2}\left(\Phi^\dagger\Phi - \frac{v^2}{2}\right) G^a_{\mu\nu} G^{a\mu\nu}, \\
O_{\Phi\tilde{G}} &= \frac{1}{2}\left(\Phi^\dagger\Phi - \frac{v^2}{2}\right) G^a_{\mu\nu} \tilde{G}^{a\mu\nu}, \\
O_{\Phi B} &= \frac{1}{2}\left(\Phi^\dagger\Phi - \frac{v^2}{2}\right) B_{\mu\nu} B^{\mu\nu}, \\
O_{\Phi\tilde{B}} &= \frac{1}{2}\left(\Phi^\dagger\Phi - \frac{v^2}{2}\right) B_{\mu\nu} \tilde{B}^{\mu\nu}, \\
O_{\Phi W} &= \frac{1}{2}\left(\Phi^\dagger\Phi - \frac{v^2}{2}\right) W^i_{\mu\nu} W^{i\mu\nu}, \\
O_{\Phi\tilde{W}} &= \frac{1}{2}\left(\Phi^\dagger\Phi - \frac{v^2}{2}\right) W^i_{\mu\nu} \tilde{W}^{i\mu\nu}, \\
O^{(1)}_{\Phi} &= \left(\Phi^\dagger\Phi - \frac{v^2}{2}\right) D_\mu \Phi^\dagger D^\mu \Phi;
\end{aligned}
\tag{1}
$$

[1]Correspondingly, a set of Schwinger-Dyson equations can be used at the quantum level.

(ii) *Scalar-fermion sector*

$$O_{t\Phi} = \left(\Phi^\dagger\Phi - \frac{v^2}{2}\right)(\bar{Q}_L\Phi^c t_R),$$
$$O_{b\Phi} = \left(\Phi^\dagger\Phi - \frac{v^2}{2}\right)(\bar{Q}_L\Phi b_R), \qquad (2)$$
$$O_{\tau\Phi} = \left(\Phi^\dagger\Phi - \frac{v^2}{2}\right)(\bar{L}_L\Phi\tau_R),$$

where the dual tensor $\tilde{F}_{\mu\nu} = \varepsilon_{\mu\nu\gamma\delta}F_{\gamma\delta}$. Deviations from the SM are defined by the effective Lagrangian

$$L_{\text{eff}}^{(6)} = \frac{1}{\Lambda^2}\sum_{k=V,F} C_{k\Phi}O_{k\Phi}, \qquad (3)$$

where the anomalous couplings C modify the SM Higgs boson couplings to the vector bosons and to the fermions.

The subtraction of $v^2/2$ leaves out undesirable mixing in the gauge field kinetic terms. Such an operator basis was considered in Ref. [7]. A reduced set of five operators for the anomalous Higgs couplings to gauge bosons only was analyzed in Ref. [8], where additional operators containing covariant derivatives of the scalar doublet ($O_W = D_\mu\Phi^\dagger D_\nu\Phi W^{\mu\nu}$ and $O_B = D_\mu\Phi D_\nu\Phi^\dagger B^{\mu\nu}$) modifying the triple gauge-boson couplings were either accepted or rejected in the two independent scenarios. The operator $O_{BW} = \Phi^\dagger\tau^a\Phi B_{\mu\nu}W^{\mu\nu}$, contributing to the $W^3 - B$ mixing of SU(2) eigenstates at the tree level is strongly constrained by the electroweak data. Mixing terms with derivatives of vector fields would imminently shift gauge boson masses, which are severely constrained by the electroweak precision data. The operator $(\Phi^+\Phi)^3$ (denoted also by $O_\Phi^{(3)}$) which shifts the minimum of the Higgs potential and the Higgs boson mass is not introduced in our analysis.

In the general case when all possible dimension-six contributions are accounted for, the effective Higgs-boson and Higgs-fermion couplings are related to the coefficients $C_{\Phi k}$ in front of the operators $O_{\Phi G}, \ldots, O_{\tau\Phi}$ in a rather nontrivial way, as a number of different coefficients $C_{\Phi k}$ mix while contributing to a single effective Higgs-boson or Higgs-fermion coupling. For the sake of distinctness we restrict the general multidimensional anomalous coupling space to the two-dimensional space,[2] where the Higgs-boson and the Higgs-fermion couplings are rescaled by independent parameters c_V and c_F. Such a reduction is also useful to avoid modifications of the Lorentz structure for a vertex. The nonzero anomalous couplings $C_{\Phi b}$ and $C_{\Phi W}$, for instance, lead to modifications of the tensor structure for HW^+W^- and HZZ vertices (see Sec. II and Table II; more details can be found in Ref. [9]). As a result, the phase-space distributions could be substantially modified [10] in comparison with the SM, making questionable the experimental interpretation of the signal reconstruction that is based specifically on the SM. A linear rescaling of the Higgs-boson and the Higgs-fermion couplings (c_V, c_F) (sometimes denoted by k_v and k_f) is a common feature of a majority of existing analyses (for a more comprehensive list see Ref. [11]) that refer to different theoretical backgrounds. A particular parametrization of the Higgs couplings of the form $k_f = \sqrt{2}(m_f/M)^{1+\varepsilon}$, $k_v = 2(m_V^{2(1+\epsilon)}/M^{1+2\varepsilon})$ (specific to the genuine Englert-Brout-Higgs spontaneous symmetry-breaking mechanism; the limiting case of the SM is $\varepsilon = 0$, $M = v$) was analyzed in Ref. [12]. One can distinguish a group of approaches where the fundamental scalar field is not a component of an SU(2) doublet [13,14]. Anomalous operators of dimension five form the corresponding effective operator basis in the framework of a nonlinear realization of the $\text{SU}(2)_L \times \text{U}(1)$ symmetry by means of an effective chiral Lagrangian. In such models the Goldstone bosons π^a are introduced in the form of a field $\Sigma(x) = \exp(i\tau^a\pi_a/v)$, which transforms linearly under the group $\text{SU}(2)_L \times \text{SU}(2)_R$. The parameter v is not a vacuum expectation value associated with a minimum of some potential; at the same time the Higgs field is an additional scalar singlet under the gauge group transformations. An effective Lagrangian in the form of an expansion in the powers of h/v can be found in Refs. [12]–[15]. The effective parameters $a, b, \ldots$ in front of the various powers of h/v in the expansion define the values of the H couplings to gauge bosons and fermions, as well as the H self-interaction. The leading operators appearing in the expansion in the inverse powers of the cutoff scale Λ have dimension five [14],

$$L_{\text{eff}}^{(5)} = -\frac{c_g g_s^2}{2\Lambda}hG_{\mu\nu}^A G^{A\mu\nu} - \frac{c_W g_2^2}{2\Lambda}hW_{\mu\nu}^a W^{a\mu\nu} - \frac{c_B g_1^2}{2\Lambda}hB_{\mu\nu}B^{\mu\nu},$$

and they are enhanced by a factor Λ/v in comparison with the effective dimension-six operators. In the minimal composite pseudo-Goldstone boson scenario the Higgs-boson and the Higgs-fermion anomalous couplings are identically rescaled, but this is not the case for nonminimal compositeness, when some higher-order chiral symmetry is broken down to the symmetry of the standard Higgs sector. A scenario where a light composite Higgs boson—emerging from a strongly interacting sector as a pseudo-Goldstone boson—causes electroweak symmetry breaking has been analysed in detail [12]–[17] in connection with LHC data. The Higgs-fermion effective terms lead to a number of observable consequences for vector-boson scattering and enhanced double Higgs boson production [15,16].

Recent updates of CMS and ATLAS results in the $\gamma\gamma$ and ZZ, WW channels [18] for the Standard Model Higgs boson allow one to improve upon previous considerations by analyzing the consistency of experimental data with the

[2] An analysis of the complete set of operators is in progress and will be presented separately.

expectations for the SM Higgs boson production. Note that these analyses are based on a phenomenological parametrization [19] specific to the production × decay approximation: when the Higgs boson width is infinitely small, the Breit-Wigner propagator is replaced by a delta function so that the signal cross section for the channel $ii \to H \to ff$ is $\sigma_{ii}(ii \to H) \times \Gamma_{ff}/\Gamma_{\rm tot}$. When "dressing" the cross sections σ_{ii} and decay widths Γ_{ff} by the scale factors $k_{i,f}$, factorizable deviations from the SM are introduced. For example, in the channel $gg \to H \to \gamma\gamma$ the anomalous factor has the simple form $k_g^2 k_\gamma^2/k_H^2$. The factors k_g and k_γ are independent parameters, i.e., vector-boson and fermion loops are not resolved.

In the following we analyze the LHC results in the framework of the SM extension by the dimension-six operators and clear up the consistency of the data with the consequences of the SM for Higgs-fermion and Higgs-gauge boson couplings.[3] The paper is organized as follows. In Sec. II a convenient normalization of the effective vertices in the dimension-six operator basis is defined. Section III contains a statistical analysis of Higgs production data. The results of our computations are summarized in Sec. IV.

II. NORMALIZATION OF EFFECTIVE VERTICES

A set of P-conserving operators [Eqs. (1) and (2)] leads to the set of Feynman rules listed in Table I.

As already mentioned in the Introduction, the following analysis will be focused on the Higgs-fermion and the Higgs-gauge boson anomalous couplings ($C_{t\Phi}$, $C_{b\Phi}$, $C_{\tau\Phi}$, $C_\Phi^{(1)}$, and $C_{\Phi G}$) which conserve the SM Lorentz structure of the vertices. It is convenient to use a parametrization which gives explicitly the SM one-loop contributions for the Higgs decays at some point of the anomalous coupling parameter space. If the effective Lagrangians for $H \to \gamma\gamma$ and $H \to gg$ are

$$L^{\rm eff}_{\gamma\gamma H} = \frac{\lambda_{\gamma\gamma H}}{4} F_{\mu\nu}F^{\mu\nu}H, \qquad L^{\rm eff}_{ggH} = \frac{\lambda_{ggH}}{4} G^a_{\mu\nu}G^{a\mu\nu}H, \quad (4)$$

respectively, then the effective vertices are

$$\Gamma^{\mu\nu}(p_1,p_2)_{\gamma/g} = -\lambda_{\gamma\gamma H/ggH}(g^{\mu\nu}p_1p_2 - p_1^\nu p_2^\mu), \quad (5)$$

where $\lambda_{\gamma\gamma H/ggH}$ are defined by the one-loop integrals. The dominant fermionic contribution of the top-quark loop leads to the well-known effective Lagrangians (see details in Ref. [21]) ($\sqrt{G_F\sqrt{2}} = 1/v$)

$$L^{\rm eff}_{\gamma\gamma H} = \frac{2\alpha}{9\pi v} F_{\mu\nu}F^{\mu\nu}H, \qquad L^{\rm eff}_{ggH} = -\frac{\alpha_s}{12\pi v} G^a_{\mu\nu}G^{a\mu\nu}H \quad (6)$$

for the case of rather small $m_H^2/4m_{\rm top}^2$, which is satisfactory[4] for $m_H = 126$ GeV. So for the top one-loop induced couplings,

$$\lambda^t_{\gamma\gamma H} = \frac{8\alpha}{9\pi v}, \qquad \lambda^t_{ggH} = -\frac{\alpha_s}{3\pi v}. \quad (7)$$

The contribution of W has been known for a long time [22],

$$\lambda^W_{\gamma\gamma H} = -\frac{7\alpha}{2\pi v}, \quad (8)$$

and the one-loop induced decay widths are [21]

$$\Gamma(H\to\gamma\gamma) = \frac{\alpha^2 G_F m_H^3}{128\pi^3\sqrt{2}}\left|3\left(\frac{2}{3}\right)^2\frac{4}{3} - 7\right|^2 = \left(\frac{47}{9}\right)^2\frac{\alpha^2 G_F m_H^3}{128\pi^3\sqrt{2}}, \quad (9)$$

$$\Gamma(H\to gg) = \frac{1}{36}\frac{\alpha^2 G_F m_H^3}{\pi^3\sqrt{2}}. \quad (10)$$

It is convenient to introduce the effective parameters

$$c_F = 1 + C_{t\Phi}\cdot\frac{v^2}{\Lambda^2},$$
$$c_V = 1 + \frac{v^2}{2\Lambda^2}\cdot C_\Phi^{(1)},$$
$$c_G = c_F + \frac{6\pi}{\alpha_s}\cdot C_{\Phi G}\cdot\frac{v^2}{\Lambda^2},$$
$$c_\gamma = \frac{63c_F - 16c_V}{47} + \frac{9\pi}{4\alpha}\cdot(c_w^2\cdot C_{\Phi B} + s_w^2\cdot C_{\Phi W})\cdot\frac{v^2}{\Lambda^2},$$
$$c_Z = (s_w^2\cdot C_{\Phi B} + c_w^2\cdot C_{\Phi W})\cdot\frac{v^2}{\Lambda^2},$$
$$c_W = C_{\Phi W}\cdot\frac{v^2}{\Lambda^2},$$

such that at the leading order the SM limit with the one-loop induced $H \to \gamma\gamma$ and $h \to gg$ channels is clearly seen.

[3] ATLAS and CMS results reported in the beginning of 2013 (Recontres de Moriond [20]) were substantially improved in May 2013 (European LC Workshop). ATLAS results in the $\gamma\gamma$ channel are as follows: significance 7.4σ, $\mu = 1.65 + 0.34 - 0.30$ (2.3σ above that expected for the SM), $m_H = 126.8 \pm 0.2({\rm stat}) \pm 0.7({\rm stat})$ GeV; ATLAS results in the ZZ channel: significance 6.6σ, $\mu = 1.70 + 0.5 - 0.4$, $m_H = 124.3 + 0.6 - 0.5({\rm stat}) + 0.5 - 0.3({\rm stat})$ GeV. CMS results in the $\gamma\gamma$ channel are as follows: significance 7σ, $\mu = 1.55 \pm 0.5$, consistent with $m_H \sim 125$ GeV; CMS results in the ZZ channel: significance 6.6σ, $\mu = 0.91 + 0.30 - 0.24$, $m_H = 125.8 \pm 0.5({\rm stat}) \pm 0.2({\rm stat})$ GeV. Improvements provided in May 2013 can be found in Sec. IV.

[4] In the numerical computations well-known formulas including $m_H^2/4m_{\rm top}^2$ terms were used.

TABLE I. Effective triple vertices in the Buchmueller-Wyler operator basis. The anomalous couplings C (Wilson coefficients) are multiplicative factors in front of O.

Effective operators	Triple vertices	Feynman rules
$O_{t\Phi} = (\Phi^\dagger\Phi - \frac{v^2}{2})(-\lambda_t)(\bar{Q}_L \Phi^c t_R)$	$\bar{t}\quad t\quad H$	$-M_t \cdot \frac{v}{\Lambda^2} \cdot C_{t\Phi}$
$O_{b\Phi} = (\Phi^\dagger\Phi - \frac{v^2}{2})(-\lambda_b)(\bar{Q}_L \Phi b_R)$	$\bar{b}\quad b\quad H$	$-M_b \cdot \frac{v}{\Lambda^2} \cdot C_{b\Phi}$
$O_{\tau\Phi} = (\Phi^\dagger\Phi - \frac{v^2}{2})(-\lambda_\tau)(\bar{L_L} \Phi \tau_R)$	$\bar{\tau}\quad \tau\quad H$	$-M_\tau \cdot \frac{v}{\Lambda^2} \cdot C_{\tau\Phi}$
$O_{\Phi G} = \frac{1}{2}(\Phi^\dagger\Phi - \frac{v^2}{2}) G^a_{\mu\nu} G^{a\mu\nu}$	$G_\mu\quad G_v\quad H$	$-2 \cdot \frac{v}{\Lambda^2} \cdot C_{\Phi G} \cdot (g^{\mu\nu} p_1 p_2 - p_1^\nu p_2^\mu)$
$O_{\Phi B} = \frac{1}{2}(\Phi^\dagger\Phi - \frac{v^2}{2}) B_{\mu\nu} B^{\mu\nu}$	$A_\mu\quad A_v\quad H$	$-2 \cdot c_w^2 \cdot \frac{v}{\Lambda^2} \cdot C_{\Phi B} \cdot (g^{\mu\nu} p_1 p_2 - p_1^\nu p_2^\mu)$
	$A_\mu\quad Z_v\quad H$	$+2 \cdot c_w \cdot s_w \cdot \frac{v}{\Lambda^2} \cdot C_{\Phi B} \cdot (g^{\mu\nu} p_1 p_2 - p_1^\nu p_2^\mu)$
	$Z_\mu\quad Z_v\quad H$	$-2 \cdot s_w^2 \cdot \frac{v}{\Lambda^2} \cdot C_{\Phi B} \cdot (g^{\mu\nu} p_1 p_2 - p_1^\nu p_2^\mu)$
$O_{\Phi W} = \frac{1}{2}(\Phi^\dagger\Phi - \frac{v^2}{2}) W^i_{\mu\nu} W^{i\mu\nu}$	$A_\mu\quad A_v\quad H$	$-2 \cdot s_w^2 \cdot \frac{v}{\Lambda^2} \cdot C_{\Phi W} \cdot (g^{\mu\nu} p_1 p_2 - p_1^\nu p_2^\mu)$
	$A_\mu\quad Z_v\quad H$	$-2 \cdot c_w \cdot s_w \cdot \frac{v}{\Lambda^2} \cdot C_{\Phi W} \cdot (g^{\mu\nu} p_1 p_2 - p_1^\nu p_2^\mu)$
	$Z_\mu\quad Z_v\quad H$	$-2 \cdot c_w^2 \cdot \frac{v}{\Lambda^2} \cdot C_{\Phi W} \cdot (g^{\mu\nu} p_1 p_2 - p_1^\nu p_2^\mu)$
	$W_\mu^+\quad W_v^-\quad H$	$-2 \cdot \frac{v}{\Lambda^2} \cdot C_{\Phi W} \cdot (g^{\mu\nu} p_1 p_2 - p_1^\nu p_2^\mu)$
$O_\Phi^{(1)} = (\Phi^\dagger\Phi - \frac{v^2}{2}) D_\mu \Phi^\dagger D^\mu \Phi$	$W_\mu^+\quad W_v^-\quad H$	$M_W^2 \cdot \frac{v}{\Lambda^2} \cdot C_\Phi^{(1)} \cdot g^{\mu\nu}$
	$Z_\mu\quad Z_v\quad H$	$M_Z^2 \cdot \frac{v}{\Lambda^2} \cdot C_\Phi^{(1)} \cdot g^{\mu\nu}$

A compact set of Feynman rules that make the triple vertices useful in the following analyses is presented in Table II. In order to take into account the next-to-leading-order (NLO) corrections, the normalization of the ggH and $\gamma\gamma H$ vertices was changed using the output of HDECAY code [23], where higher-order QCD and leading electroweak corrections from different sources have been incorporated. For example, the effective coupling constants $\lambda_{\gamma\gamma H}$ and $\lambda_{\gamma ZH}$ can be found using partial widths,

$$\lambda_{\gamma\gamma H} = 8\sqrt{\frac{\pi}{m_H^3}\Gamma^{\rm tot}\mathrm{Br}(H\to\gamma\gamma)},$$
$$\lambda_{\gamma ZH} = 8\sqrt{\frac{\pi m_H^3}{2(m_H^2 - m_Z^2)^3}\Gamma^{\rm tot}\mathrm{Br}(H\to\gamma Z)}. \quad (11)$$

TABLE II. Triple vertices in the Buchmueller-Wyler operator basis. The SM limit with the one-loop induced vertices $H\to\gamma\gamma$ and $h\to gg$ is achieved at $c_V = c_F = c_G = c_\gamma = 1$, $c_Z = c_W = C_{\Phi B} = C_{\Phi W} = 0$.

Triple vertices	Feynman rules
$\bar{t}\quad t\quad H$	$-\frac{M_t}{v}\cdot c_F$
$\bar{b}\quad b\quad H$	$-\frac{M_b}{v}\cdot c_F$
$\bar{\tau}\quad \tau\quad H$	$-\frac{M_\tau}{v}\cdot c_F$
$G_\mu\quad G_\nu\quad H$	$-\frac{2}{v}\cdot\frac{\alpha_s}{6\pi}\cdot c_G\cdot(g^{\mu\nu}p_1p_2 - p_1^\nu p_2^\mu)$
$A_\mu\quad A_\nu\quad H$	$-\frac{2}{v}\cdot\frac{4\alpha}{9\pi}\cdot c_\gamma\cdot(g^{\mu\nu}p_1p_2 - p_1^\nu p_2^\mu)$
$A_\mu\quad Z_\nu\quad H$	$+2\cdot c_w\cdot s_w\cdot(C_{\Phi B} - C_{\Phi W})\cdot\frac{v}{\Lambda^2}(g^{\mu\nu}p_1p_2 - p_1^\nu p_2^\mu)$
$Z_\mu\quad Z_\nu\quad H$	$+\frac{2}{v}\cdot[M_Z^2\cdot c_V\cdot g^{\mu\nu} - c_Z\cdot(g^{\mu\nu}p_1p_2 - p_1^\nu p_2^\mu)]$
$W_\mu^+\quad W_\nu^-\quad H$	$+\frac{2}{v}\cdot[M_W^2\cdot c_V\cdot g^{\mu\nu} - c_W\cdot(g^{\mu\nu}p_1p_2 - p_1^\nu p_2^\mu)]$

Such a normalization reproduces the SM limit at $c_i = 1$, $i = F,\ V,\ G,\ \gamma,\ c_Z = c_W = 0$. The one-loop vertices are "resolved" at the leading order. For example, destructive interference between the top and W loops [see Eqs. (7) and (8)] leads to an enhancement in the $\gamma\gamma$ channel at negative c_F, where an extensive region compatible with the data appears (see Sec. IV). However, NLO corrections from anomalous dimension-six terms inside the loops are not accounted for.

III. SIGNAL STRENGTH AND EXCLUSION CONTOURS IN THE SPACE OF ANOMALOUS PARAMETERS

The method of exclusion contour reconstruction in the relevant anomalous parameter space that we are using is similar to the method developed in Refs. [17,24]. Available experimental data provides the signal strength,

$$\mu_i = \frac{[\Sigma_j \sigma_{j\to h}\mathrm{Br}(h\to i)]_{\rm obs}}{[\Sigma_j \sigma_{j\to h}\mathrm{Br}(h\to i)]_{\rm SM}}, \quad (12)$$

where i is the number of Higgs boson decay channels and j is the number of Higgs production processes for a given final state. The best-fit value of the signal strength can be expressed using the observed number of signal events $N_{\rm obs}$, the number of background events $N_{\rm backgr}$, and the number of signal events calculated in the SM $N^{\rm SM}_{\rm signal}$,

$$\hat{\mu}_i = \frac{N_{{\rm obs},i} - N_{{\rm backgr},i}}{N^{\rm SM}_{{\rm signal},i}}. \quad (13)$$

The global χ^2 is defined as

$$\chi^2(\mu_i) = \sum_i^{N_{\rm ch}} \frac{(\mu_i - \hat{\mu}_i)^2}{\sigma_i^2} \tag{14}$$

for the number of production channels $N_{\rm ch}$. Theoretical predictions for $\sigma_{j\to h}$ and related errors are published by the LHC Higgs Cross Section Working Group [25]. The minimization of $\chi^2 \to \chi^2_{\rm min}$ gives us the 1σ, 2σ, and 3σ regions with $\chi^2 = \chi^2_{\rm min} + \Delta\chi^2$, where $\Delta\chi^2$ is defined by a cumulative distribution function. Assuming that the signal strengths of various channels have Gaussian distributions, that the probability density functions (PDFs) having the expected values $\hat{\mu}_i$, and that the dispersions (1σ deviations) σ_i are normalized to one, the combined PDF for a number of production channels can be found by multiplying the PDFs for the individual channels. The combined probability density function is also Gaussian and is characterized by μ_c and σ_c,

$$\frac{1}{\sigma_c^2} = \sum_i^{N_{\rm ch}} \frac{1}{\sigma_i^2}, \qquad \frac{\hat{\mu}_c}{\sigma_c^2} = \sum_i^{N_{\rm ch}} \frac{\hat{\mu}_i}{\sigma_i^2} \tag{15}$$

which allows one to determine, for example, the 95% C.L. exclusion upper μ_U and lower μ_L limits on the signal strength parameter by integrating the combined PDF from $\hat{\mu}$ to μ_U and from μ_L to $\hat{\mu}$, respectively, and then equating the result to $0.95/2$. Possible negative values of the lower limit for the signal strength at small luminosities allows one to determine only μ_U by integrating the probability density function from 0 to μ_U and equating it to 0.95.

If the SM is fully adequate, the values of μ_i are as close to 1 as allowed by experimental errors. In the framework of the SM extension by dimension-six effective operators the values of μ_i obviously may depart from 1 for individual channels, so it is convenient to normalize the signal strengths (13) to the expectation values in the given SM extension, $N_{{\rm signal},i,c_F,c_V,c_W\ldots}$, rather than the SM expectation, $N^{\rm SM}_{{\rm signal},i}$, which does not depend on the anomalous parameters $c_F, c_V, c_W, \ldots$. In this case the combined signal strength with expectation 1 can be introduced again if the exclusion bounds $\hat{\mu}_i \pm \sigma_i$ are renormalized by a factor $N^{\rm SM}_{{\rm signal},i}/N_{{\rm signal},i,c_F,c_V,c_W\ldots}$. While the experimental signal strength error is provided by the ATLAS and CMS collaborations, the theoretical signal strength error is evaluated using numbers from the LHC Higgs Cross Section Working Group [25].

In the following fits we use the signal strength calculated at $m_H = 125$ GeV. At the first stage a two-dimensional fit $\chi^2(c_V, c_F)$ is performed and the anomalous couplings $C_{\Phi B}$ and $C_{\Phi W}$ (see Sec. II) are taken to be zero, so for the SM case $(c_V, c_F) = (1, 1)$, $c_G = c_\gamma = 1$ and $c_Z = c_W = 0$. The calculation of the $\Delta\chi^2$ for the best fit defines a given number × C.L. contour corresponding to the departure of the SM point (1, 1) from the best-fit point in the (c_V, c_F) parameter plane. Following Ref. [17], the contours in all figures correspond to 65%, 90%, and 99% best-fit C.L. regions with $\Delta\chi^2$ less than 2.10, 4.61, and 9.21, respectively.

IV. BEYOND THE INFINITELY SMALL WIDTH APPROXIMATION

Calculations of complete gauge-invariant sets of diagrams—although complicated and CPU time consuming—are more precise than the production × decay approximation. They take into account the following factors.

(i) Nontrivial interference between signal diagrams. For example, the four-lepton final states $l^+l^-l^+l^-$ and/or $\nu_l\nu_l l^+l^-$ are produced through $H \to Z^*Z^*$, $H \to W^*W^*$, and $\gamma\gamma$ intermediate states (see Figs. 1 and 2) with nontrivial interferences, which are not accounted for in the production × decay approximation.

(ii) Nontrivial interference between the signal and the irreducible background diagrams. Although it is very small for narrow-width resonances of the order of a few MeV, in the meaningful regions of the anomalous coupling space the anomalous Higgs boson width differs by around one order of magnitude from the SM total width. Numerical results for complete tree-level sets are in some cases sensitive to Breit-Wigner propagators, especially when strong gauge cancellations between diagrams take place for a given Higgs production channel.

(iii) Lepton and jet distributions, calculated at complete tree level, are based on correct kinematics, which are often not available for the production × decay approximation. Correct distributions are important in a real experimental environment where detector acceptances must be accounted for.

Some theoretical issues and numerical examples concerning these factors were analyzed for LEP2 physics [26].

A number of exclusion contours were reconstructed using the statistical approach described in Sec. III. The following Higgs production processes have been calculated.

(i) $\gamma\gamma$ event signature: Gluon fusion $gg \to \gamma\gamma$, vector-boson fusion (VBF) $qq \to qq\gamma\gamma$, the associated production with vector bosons $qq \to W\gamma\gamma$, $qq \to Z\gamma\gamma$, and the top-antitop quark pair $qq \to t\bar{t}\gamma\gamma$. Contributions to the Higgs boson production rate involving Higgs couplings to c and b quarks—such as diagrams with intermediate Higgs in the processes $c\bar{c} \to \gamma\gamma$ and $b\bar{b} \to \gamma\gamma$ and diagrams with the Higgs radiation from c and b quark lines in the associated production with W, Z and $t\bar{t}$ (for example, $\bar{s}c \to W^+\gamma\gamma$, $s\bar{c} \to W^-\gamma\gamma$, six diagrams)—give a very small yield, and for this reason they are omitted. Only the gauge-invariant subset of eight diagrams with Higgs boson radiation from the top line $gg \to \gamma\gamma t\bar{t}$ is calculated, omitting the 18 diagrams with different topologies. Being marginally

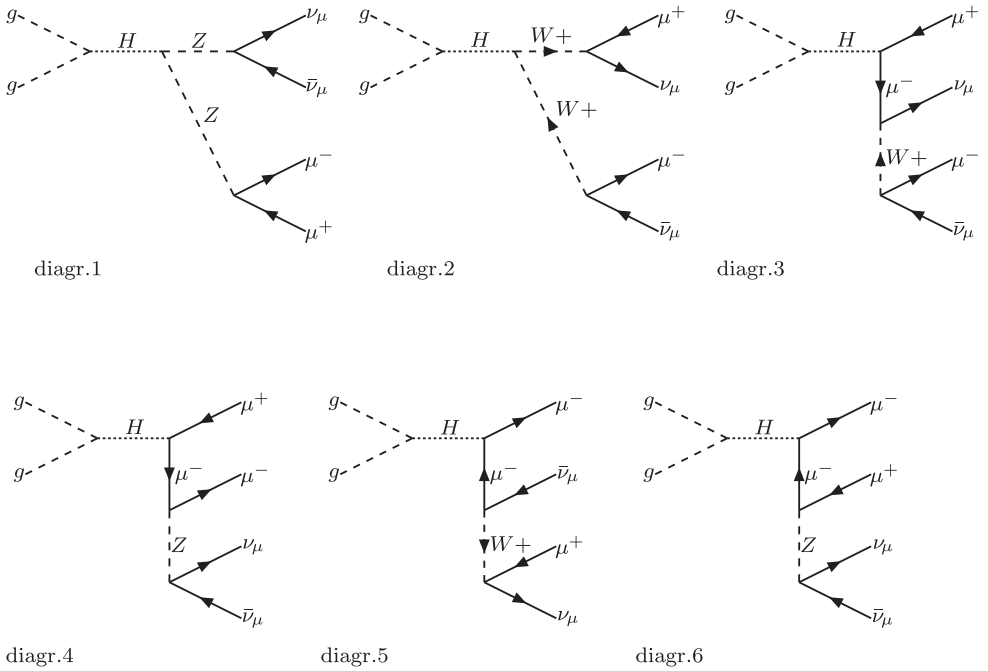

FIG. 1. Signal diagrams for the process $gg \to WW \to \nu_e \bar{\nu}_e e^+ e^-$.

small in the SM, such amplitudes could give substantial contributions in the anomalous coupling space. We checked explicitly the absence of anomalous enhancements. 20 partonic subprocesses $q\#q\# \to q\#q\#\gamma\gamma$ were accounted for in the VBF channel, including interference terms between the diagrams. The notation $q\#$ is used to account for all possible combinations of u, d, c, s quarks and antiquarks.

(ii) Event signatures with four leptons $gg \to \nu_l \bar{\nu}_l l^+ l^-$ and $gg \to l^+ l^- l^+ l^-$ including interference terms between $H \to W^+W^-$ and $H \to ZZ$: The vector boson channels $H \to W^+W^-$ and $H \to ZZ$ usually mix. A complete set of six Higgs production diagrams in the channel $pp \to WW \to \nu_\mu \bar{\nu}_\mu \mu^+ \mu^-$ (WW production via gluon fusion) is shown in Fig. 1: contributions come from diagram 2 (accounted for in the production × decay decay approximation), the $H \to ZZ$ channel (diagram 1), and the four s-channel amplitudes (diagrams 4–6), as well as interference terms, which are rather small in this case. In this channel the WW^*-ZZ^* interference term is negative (the value is of the order of a few percent, in comparison with $|WW^*|^2 + |ZZ^*|^2$), which cancels the yield of the $|ZZ^*|^2$ term. Leptonic event signatures in WW and ZZ VBF processes were included in the $(2 \to 4) \times (1 \to 2)$ infinitely small width approximation, which can be justified by their smaller significance in comparison with $\gamma\gamma$ VBF. One more example for the $ZZ \to \mu^+\mu^-\mu^+\mu^-$ channel is shown in Fig. 2, where the "exchange" interference term ZZ^*-ZZ^* is positive with a magnitude of approximately 20% of the $|ZZ^*|^2$ term. Diagrams with intermediate photons contribute insignificantly in the anomalous coupling space. As one could expect, the amplitudes with a triple Higgs vertex (diagram 9) and t-channel gluon exchange (diagram 10) were found to be insignificant for the fit in the vicinity of the SM point.

(iii) Event signatures with $b\bar{b}$ and $\tau^+\tau^-$: For $H \to b\bar{b}$ the processes $q_1\bar{q}_2 \to Wb\bar{b}$ and $q\bar{q} \to Zb\bar{b}$ were calculated. Again, diagrams with Higgs boson radiation from c and b quark lines were neglected. For the $H \to \tau^+\tau^-$ channel we calculated $\tau^+\tau^-$, $\tau^+\tau^-$ VBF, $\tau^+\tau^- t\bar{t}$, $\tau^+\tau^- W$, and $\tau^+\tau^- Z$ production.

In order to validate our codes and numerical fitting procedures we reproduce the global fit of the first paper in Ref. [17], which was reconstructed in the (a, c) plane on the basis of 2012 post-Moriond data in the infinitely small width (ISW) approximation [compare Fig. 3(a) and Fig. 3(b)]. Our contours in the (c_V, c_F) plane were also generated in the ISW approximation. For example, when considering the process $pp \to \nu_\mu \bar{\nu}_\mu \mu^+ \mu^-$ within the ISW approximation the $2 \to 3$ process $pp \to Z\mu^+\mu^-$ is calculated on a 31×31 grid in the (c_V, c_F) plane, which is then convoluted with the branching $Z \to \mu^+\mu^-$ calculated on the same grid.[5] Figure 4 shows good agreement in the ISW approximation for the three groups of channels with (a) $H \to \gamma\gamma$ in the final state, (b) $H \to WW^*$ and $H \to ZZ^*$, and (c) $H \to b\bar{b}$ and $H \to \tau^+\tau^-$.

[5]A special regime of "table calculations" (numerical operations with multidimensional tables) has been implemented in CompHEP version 4.5 [27].

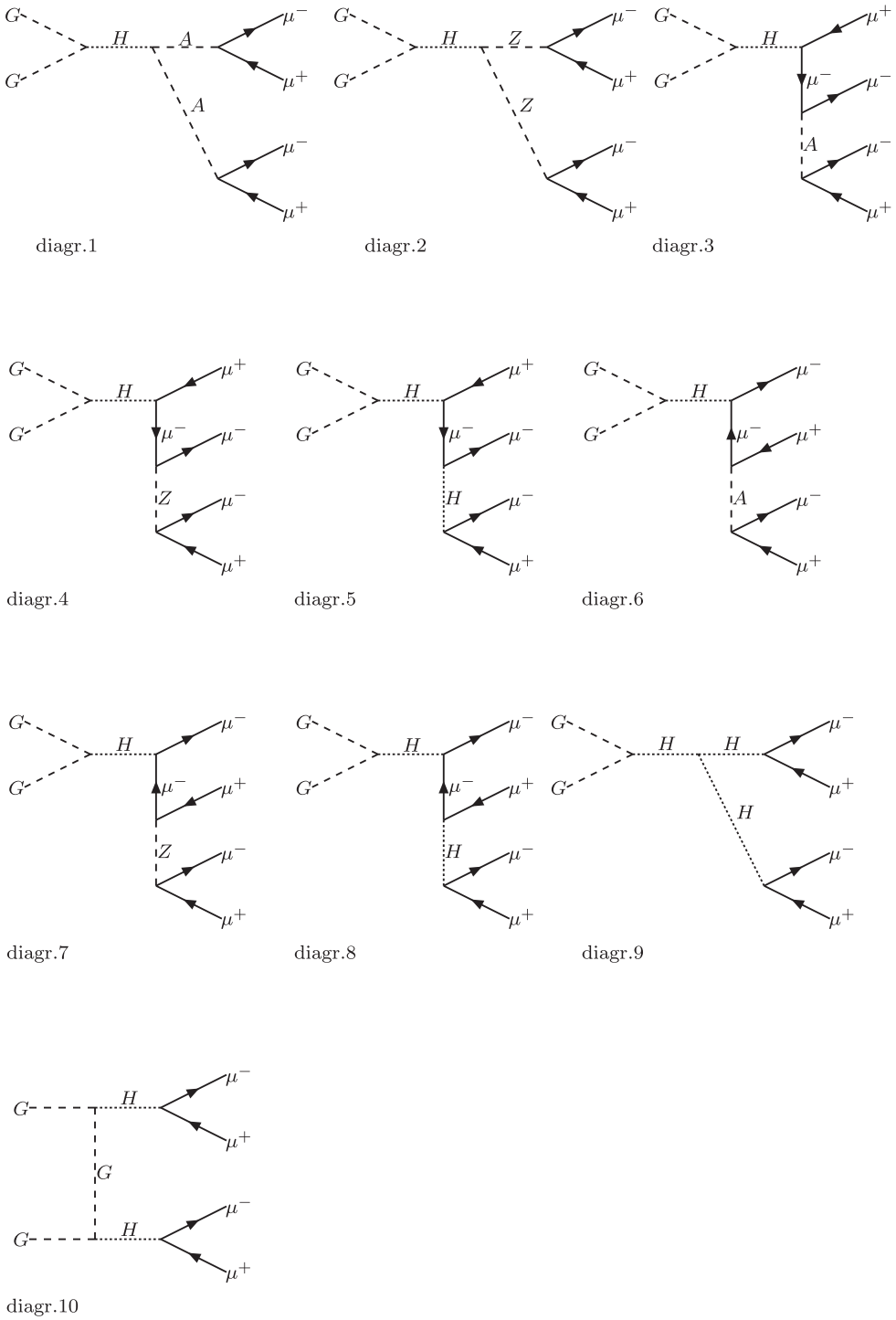

FIG. 2. Signal diagrams for the process $gg \to ZZ \to \mu^+\mu^-\mu^+\mu^-$.

According to Fig. 3 the data is consistent with the standard Higgs-sector hypothesis at the 82% C.L. The symmetry $c_F \to -c_F$ for preferable regions in the (c_V, c_F) plane is violated not only by loop corrections but also beyond the infinitely small width approximation, where a number of additional diagrams and interference terms appear. For example, when the above-mentioned $pp \to \nu_\mu \bar{\nu}_\mu \mu^+ \mu^-$ is calculated beyond the ISW as a $2 \to 4$ process at complete tree level, $H \to ZZ \to \nu_\mu \bar{\nu}_\mu \mu^+ \mu^-$ and $H \to W^+W^- \to \nu_\mu \bar{\nu}_\mu \mu^+ \mu^-$ interfere with each other (see Fig. 1) and they both contribute. Figure 5 demonstrates the visible deviations of the exclusion contours for the above-mentioned group (ii). An important additional source of deviation could be diagrams with gluon fusion (gluons radiating from the quark lines). The role of such diagrams is illustrated separately in Fig. 6. Gluon fusion—

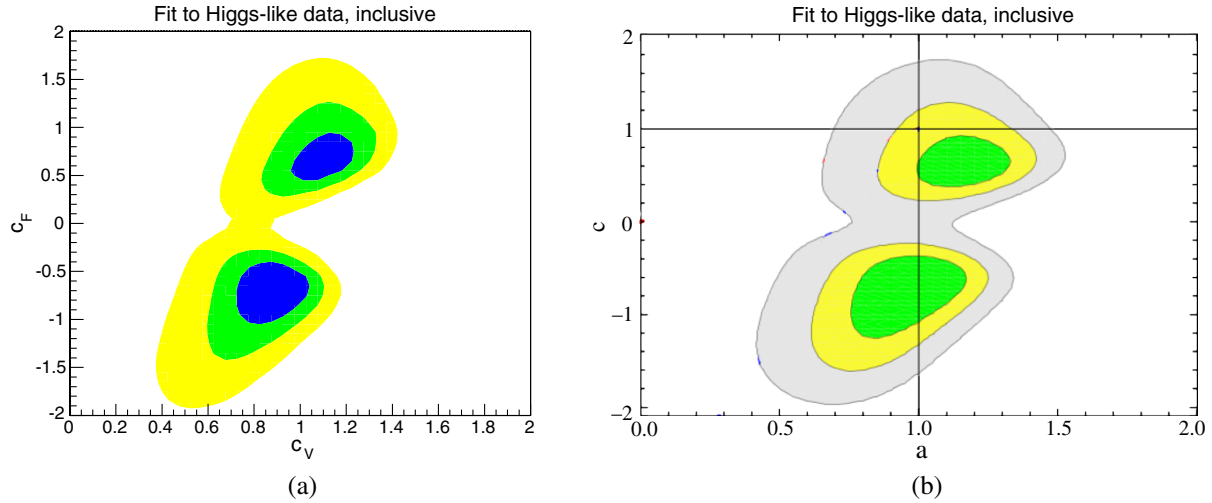

FIG. 3 (color online). (a) Global χ^2 fit in the (c_V, c_F) plane calculated with Higgs boson width for all two-particle, WW^* and ZZ^* decay channels including VBF (diagrams with gluon fusion omitted) combined with $\gamma\gamma$ VBF, within the production × decay approximation. (b) Global χ^2 fit in the (a, c) plane from Ref. [17].

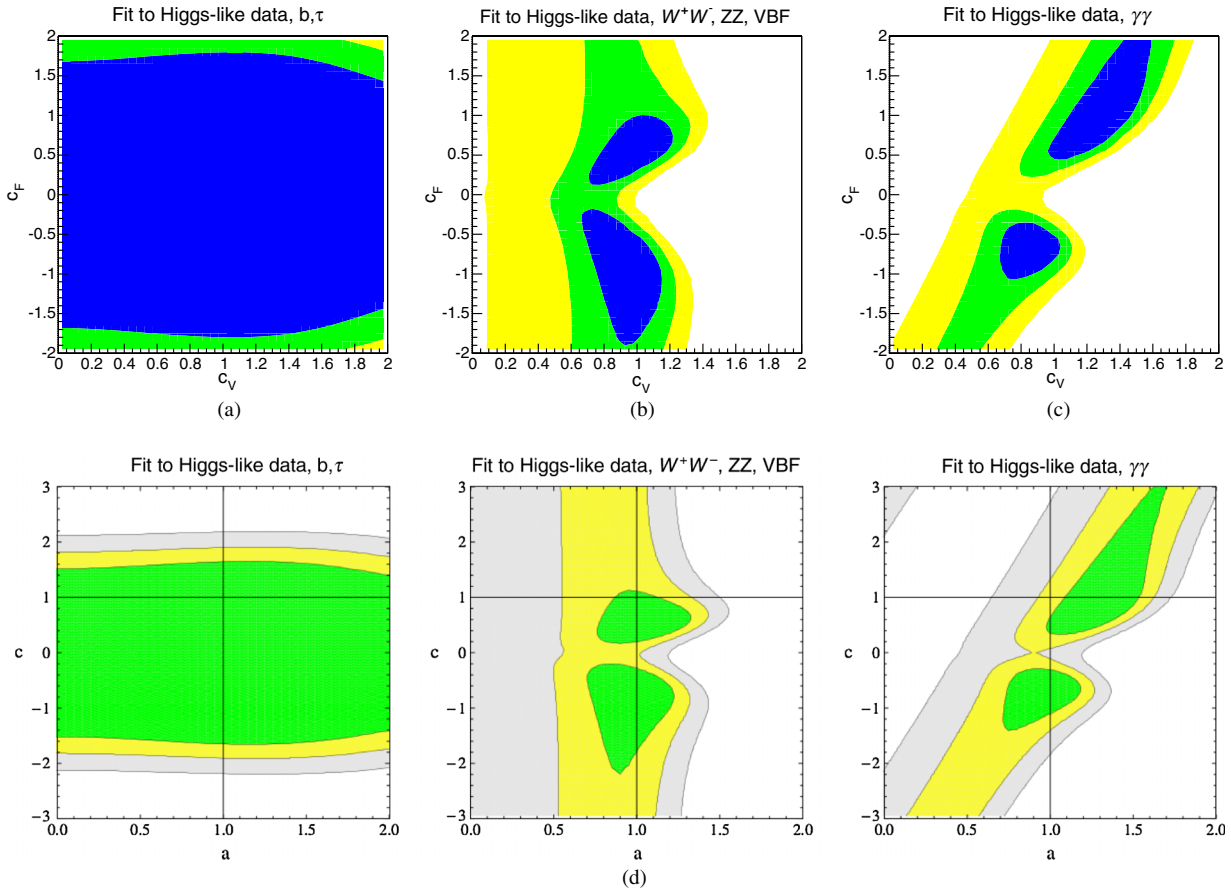

FIG. 4 (color online). χ^2 fits in the (c_V, c_F) plane calculated within the production × decay approximation. (a) $b\bar{b}$ and $\tau^+\tau^-$ channels; (b) WW^* and ZZ^* channels including VBF (diagrams with gluon fusion omitted) combined with $\gamma\gamma$ VBF; (c) $\gamma\gamma$ channels including VBF; (d) the same fits for the $b\bar{b}$, $\tau^+\tau^-$, WW^*, ZZ^*, and $\gamma\gamma$ channels in the (a, c) plane from Ref. [17]. Note that different ranges for c_F are used in the upper and lower rows of plots.

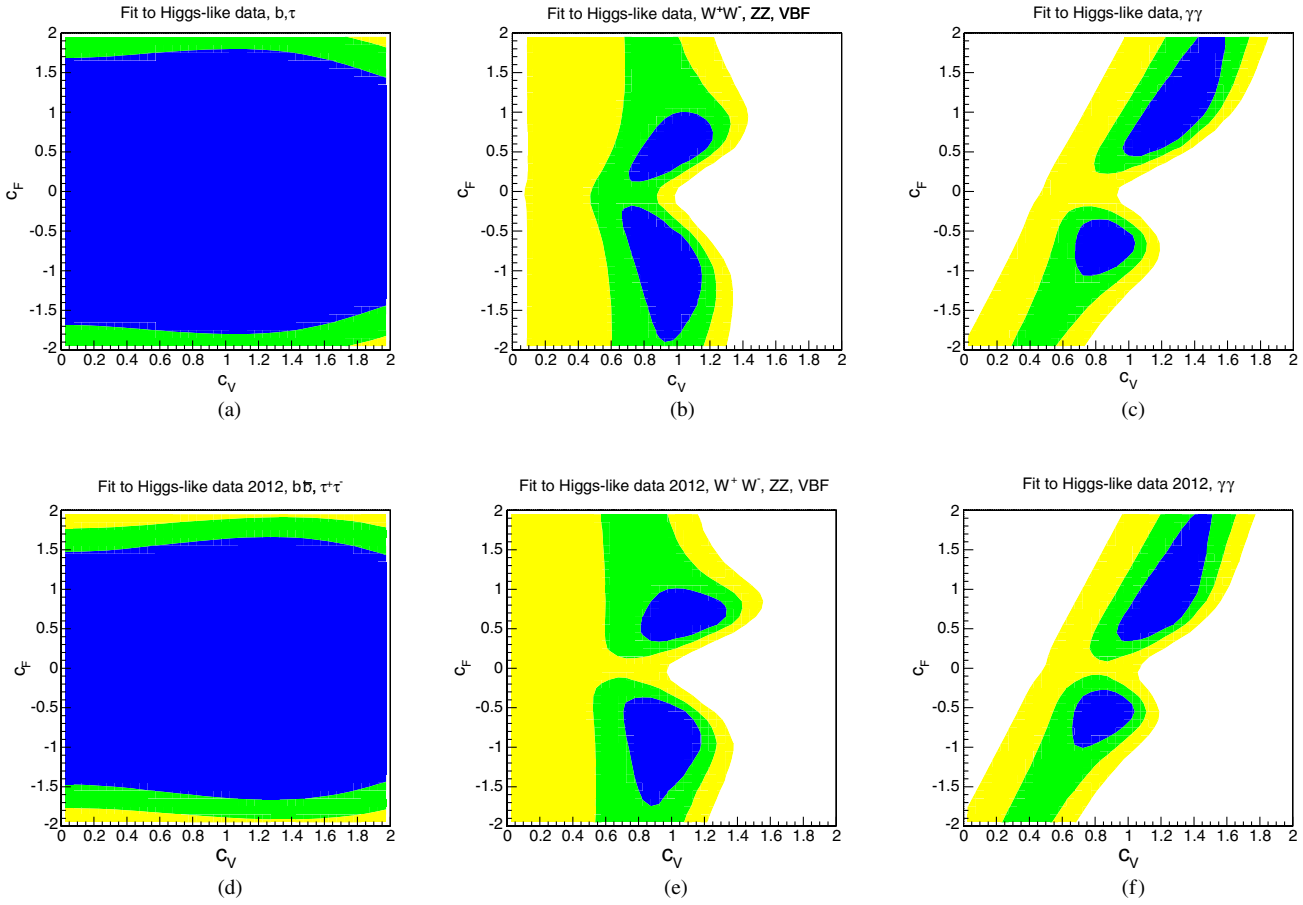

FIG. 5 (color online). (a), (b), and (c): χ^2 fits (2012 data) in the (c_V, c_F) plane calculated within the production × decay approximation. (d), (e), and (f): The same fits calculated with complete gauge-invariant sets of diagrams. (a) and (d): $b\bar{b}$ and $\tau^+\tau^-$ channels; (b) and (e): WW^* and ZZ^* channels including VBF (diagrams with gluon fusion omitted) combined with $\gamma\gamma$ VBF; (c) and (f): $\gamma\gamma$ channels including VBF.

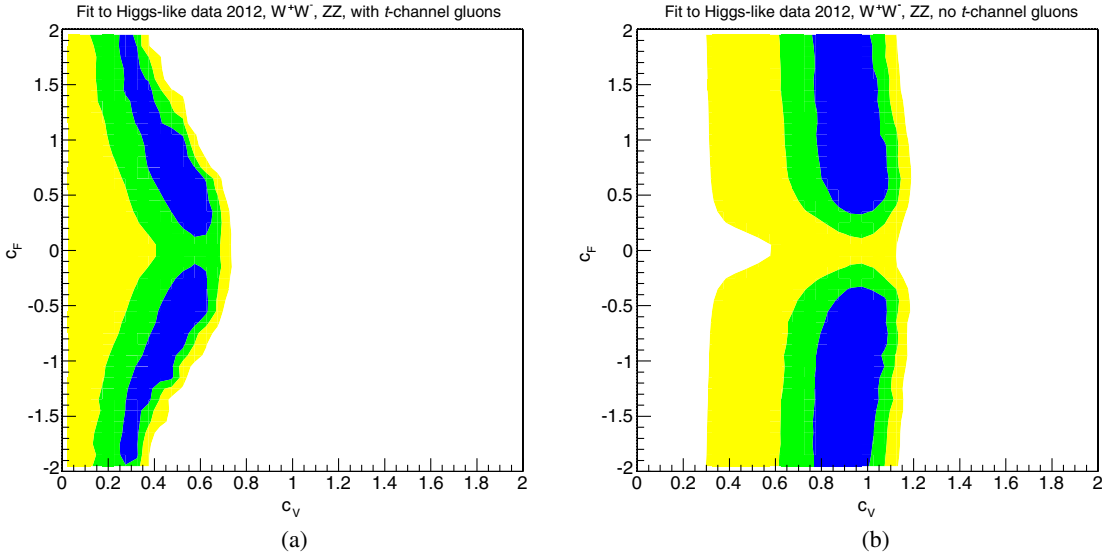

FIG. 6 (color online). χ^2 fits in the (c_V, c_F) plane calculated for the WW^* and ZZ^* channels including VBF (ladder) diagrams with the fusion of gluons radiated from the quark lines (a) and with the intermediate gluons omitted (b). Identical signal strengthes and signal strength errors were taken for the four-lepton final states produced either without forward jets or with forward jet tagging. $\gamma\gamma$ VBF diagrams are not accounted for.

TABLE III. The signal strength and the signal strength error following Ref. [28].

channel	ATLAS	CMS
$VH \to Vb\bar{b}$	-0.4 ± 1.0	1.15 ± 0.62
$H \to \tau^+\tau^-$	0.8 ± 0.7	1.10 ± 0.41
$H \to WW^*$	1.0 ± 0.3	0.68 ± 0.20
$H \to ZZ^*$	1.5 ± 0.4	0.92 ± 0.28
$H \to \gamma\gamma$	1.6 ± 0.3	0.77 ± 0.27

accounted for in the Q^2 evolution of the parton distribution functions for the fully inclusive processes—deserves careful evaluation if some specific selection criteria for the forward jets are used. In our evaluations we omit gluon-fusion amplitudes.

The relevance of VBF in the $H \to \gamma\gamma$ channel is demonstrated in Fig. 8 (upper row of plots). In the three-dimensional plot $\sigma(c_V, c_F)$ the surfaces of the VBF cross section and the cross section of processes without forward jets have opposite behavior (while one is increasing, the other is decreasing), with the result being that the exclusion contour is very sensitive to the precision of the evaluations.

The latest data from LC2013 [28] are presented in Table III. Significant improvements in precision have been achieved for the $b\bar{b}$ and $\tau^+\tau^-$ channels. In the 2012 data the signal strength error for both ATLAS and CMS was about 2, with a decrease by a factor of 3–4 reported at the beginning of 2013. Improvements for the WW, ZZ, and inclusive $\gamma\gamma$ channels have also been quite substantial, reducing the signal strength error by approximately a factor of 2. The $H \to W^+W^-$ signal strength reported by ATLAS was reduced to 1. The CMS signal strength for the $\gamma\gamma$ channel was reported at the level of 0.77 in 2013, compared with 1.6 in the earlier data processing. ATLAS reduced this figure from 1.8 to 1.6. Some improvement for the VBF $\gamma\gamma$ channel was found. A new result for the signal strength of 1.1 using the reduced error in the $\tau^+\tau^-$ channel achieved by CMS improves upon the primary value of 0.7. The contours generated with post-Moriond 2012 and preliminary LC2013 data for the three groups of channels [(i), (ii), and (iii); see above] are shown in Fig. 7. As a result, the area at negative c_F disappears almost completely, while the contours of the positive (c_V, c_F) quadrant are consistent with the SM hypothesis at the level of 95%. These modifications are in qualitative agreement with the global combination from Ref. [29], which is based on Moriond 2013 experimental data [30].

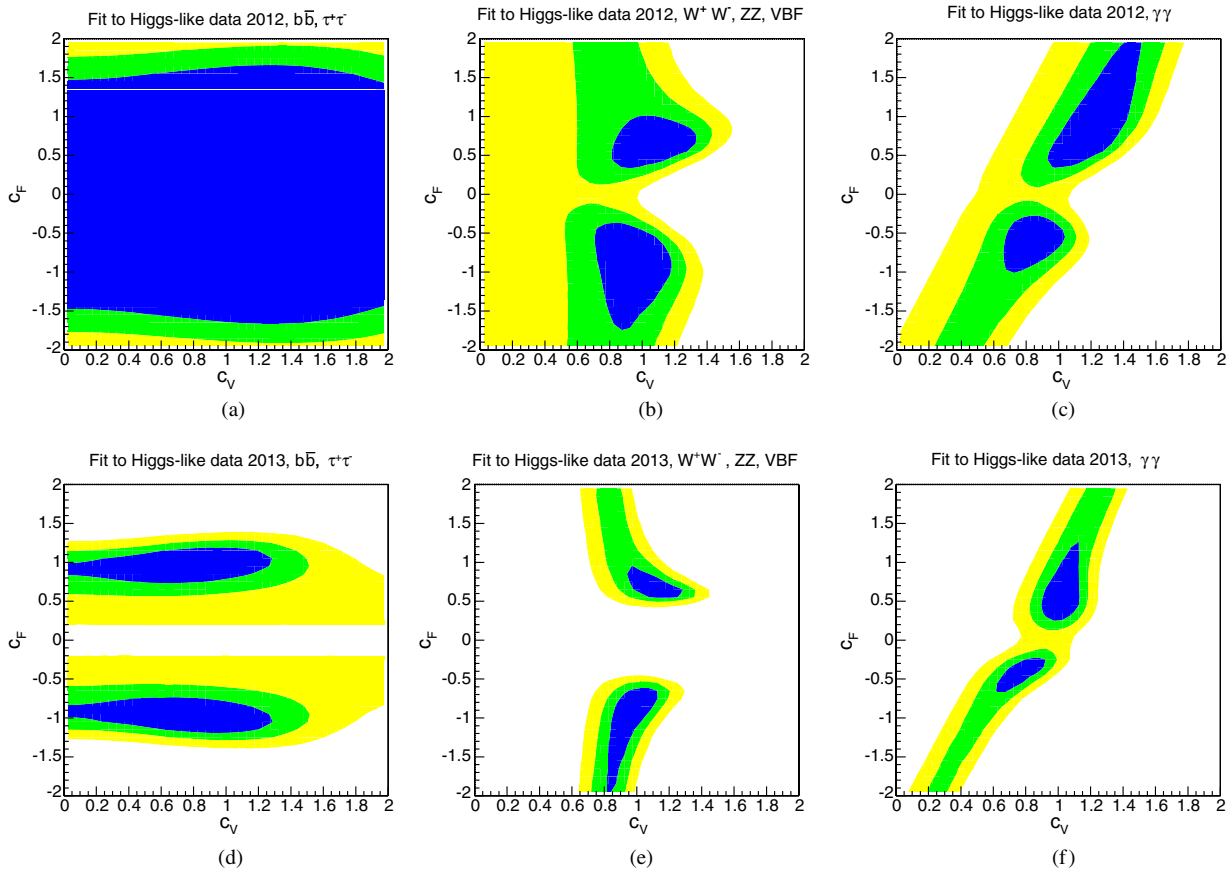

FIG. 7 (color online). (a), (b), and (c): χ^2 fits in the (c_V, c_F) plane calculated using post-Moriond 2012 data. (d), (e), and (f): The same fits calculated using LC2013 data (see Table III). (a) and (d): $b\bar{b}$ and $\tau^+\tau^-$ channels; (b) and (e): WW^* and ZZ^* channels (including VBF) combined with $\gamma\gamma$ VBF; (c) and (f): $\gamma\gamma$ channels including VBF.

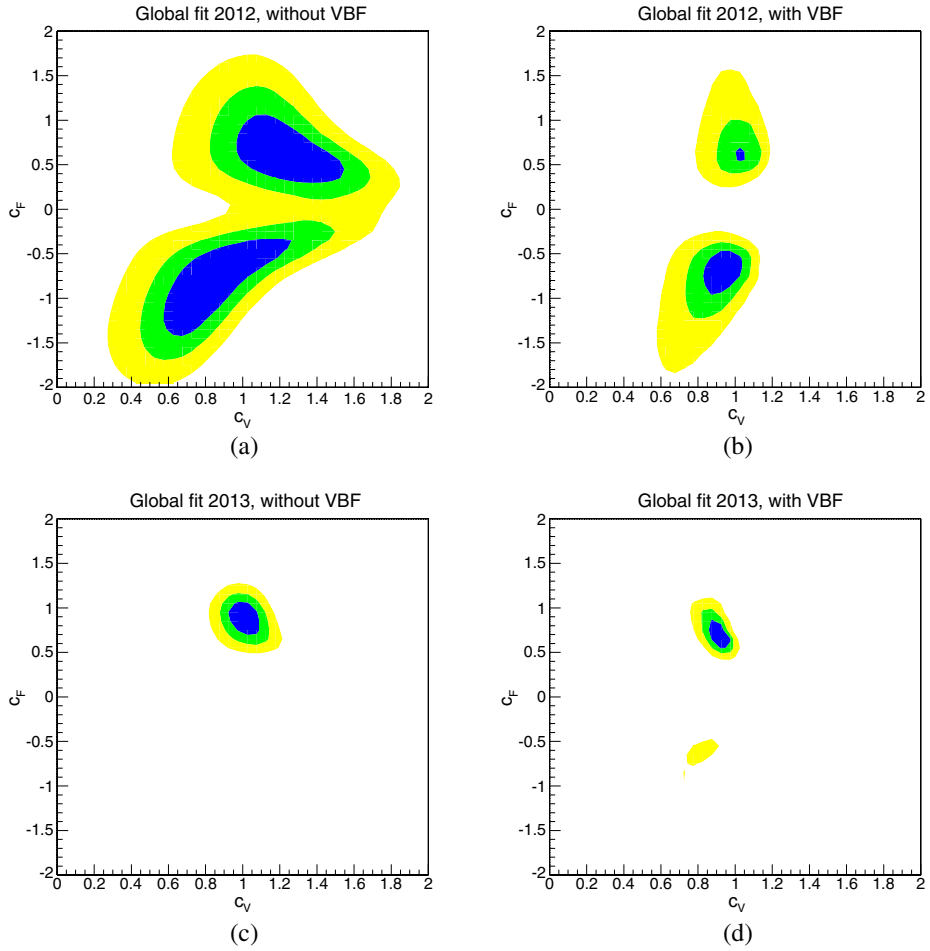

FIG. 8 (color online). Global χ^2 fits in the (c_V, c_F) plane calculated without VBF diagrams in the $\gamma\gamma$, WW^* and ZZ^* channels [(a) and (c)] and calculated with VBF diagrams in the $\gamma\gamma$, WW^* and ZZ^* channels [(b) and (d)]. (a) and (b) are based on 2012 data, whereas (c) and (d) are based on preliminary 2013 data (Table III).

V. CONCLUSIONS

The LHC data in various channels of Higgs boson production have been analyzed in the framework of the Standard Model extension by the dimension-six effective operators. In order to understand the consistency between the consequences of the SM and the experimental data a number of global fits for the signal strengths in various channels was performed and the exclusion regions in the (c_V, c_F) anomalous coupling plane were reconstructed using post-Moriond 2012 data and recent LC2013 data. In agreement with Ref. [17], two best-fit regions were found for positive and negative values of c_F, demonstrating the consistency of the SM hypothesis with the post-Moriond 2012 data at the level of 82%. In the infinitely small width approximation (or production × decay approximation) we produced results that are practically identical to those of Ref. [17], although different physics frameworks (effective operator bases) for the rescaling of the Higgs-boson and the Higgs-fermion couplings were used in the analyses. Evaluations beyond the infinitely small width approximation demonstrate visible departures of the exclusion contours for the combination of $H \to W^+W^-$, ZZ, and $\gamma\gamma$ channels, however they are insignificant for the global fits. Improvements of the precision achieved in 2013 [28] excluded practically completely the region with negative values of c_F, showing the consistency of the SM hypothesis with the 2013 data at the level of 95%.

ACKNOWLEDGMENTS

The work of E. B., V. B., and M. D. was partially supported by RFBR Grant No. 12-02-93108 and NSh Grant No. 3042.2014.2. M. D. is grateful to Andre David for useful discussion.

[1] G. Aad *et al.* (ATLAS Collaboration), Phys. Lett. B **716**, 1 (2012); S. Chatrchyan *et al.* (CMS Collaboration), *ibid.* **716**, 30 (2012).

[2] E. Eichten, K. Lane, and M. Peskin, Phys. Rev. Lett. **50**, 811 (1983); H. Weldon and A. Zee, Nucl. Phys. **B173**, 269 (1980).

[3] K. Whisnant, J. M. Yang, B.-L. Young, and X. Zhang, Phys. Rev. D **56**, 467 (1997); S. Dimopoulos, and J. Ellis, Nucl. Phys. **B182**, 505 (1981); R. Cahn and H. Harari, Nucl. Phys. **B176**, 135 (1980); Y. Maehara and T. Yanagida, Prog. Theor. Phys. **61**, 1434 (1979).

[4] W. Buchmuller and D. Wyler, Nucl. Phys. **B268**, 621 (1986).

[5] B. Grzadkowski, M. Iskrzynski, M. Misiak, and J. Rosiek, J. High Energy Phys. 10 (**2010**) 085.

[6] R. Contino, M. Ghezzi, C. Grojean, M. Muhlleitner, and M. Spira, J. High Energy Phys. 07 (**2013**) 035.

[7] G. Passarino, Nucl. Phys. **B868**, 416 (2013).

[8] T. Corbett, O. J. P. Eboli, J. Gonzalez-Fraile, and M. C. Gonzalez-Garcia, Phys. Rev. D **86**, 075013 (2012).

[9] B. Dumont, S. Fichet, and G. von Gersdorff, J. High Energy Phys. 07 (**2013**) 065.

[10] S. Banerjee, S. Mukhopadhyay, and B. Mukhopadhyaya, arXiv:1308.4860 [Phys. Rev. D (to be published)].

[11] W.-F. Chang, W.-P. Pan, and F. Xu, Phys. Rev. D **88**, 033004 (2013); K. Cheung, J. S. Lee, and P.-Y. Tseng, J. High Energy Phys. 05 (**2013**) 134; G. Belanger, B. Dumont, U. Ellwanger, J. F. Gunion, and S. Kraml, *ibid.* 02 (**2013**) 053; A. Azatov and J. Galloway, Int. J. Mod. Phys. A **28**, 1330004 (2013); T. Corbett, O. J. P. Eboli, J. Gonzalez-Fraile, and M. C. Gonzalez-Garcia, Phys. Rev. D **87**, 015022 (2013); E. Masso and V. Sanz, *ibid.* **87**, 033001 (2013); S. Dittmaier and M. Schumacher, Prog. Part. Nucl. Phys. **70**, 1 (2013); G. Cacciapaglia, A. Deandrea, G. Drieu La Rochelle, and J.-B. Flament, J. High Energy Phys. 03 (**2013**) 029; B. Dobrescu and J. Lykken, *ibid.* 02 (**2013**) 073; B. Batell, S. Gori, and L.-T. Wang, *ibid.* 01 (**2013**) 139; A. Djouadi, arXiv:1208.3436; T. Plehn and M. Rauch, Europhys. Lett. 100, **11020** (2012); F. Bonnet, T. Ota, M. Rauch, and W. Winter, Phys. Rev. D **86**, 093014 (2012); S. Banerjee, S. Mukhopadhyay, and B. Mukhopadhyaya, J. High Energy Phys. 10 (**2012**) 062; D. Carmi, A. Falkowski, E. Kuflik, T. Volansky, and J. Zupan, *ibid.* 10 (**2012**) 196; M. Montull and F. Riva, *ibid.* 11 (**2012**) 018; P. Giardino, K. Kannike, M. Raidal, and A. Strumia, Phys. Lett. B **718**, 469 (2012); I. Low, J. Lykken, and G. Shaughnessy, Phys. Rev. D **86**, 093012 (2012); M. Klute, R. Lafaye, T. Plehn, M. Rauch, and D. Zerwas, Phys. Rev. Lett. **109**, 101801 (2012); A. Azatov, R. Contino, D. Del Re, J. Galloway, M. Grassi, and S. Rahatlou, J. High Energy Phys. 06 (**2012**) 134; T. Li, X. Wan, Y.-k. Wang, and S.-h. Zhu, *ibid.* 09 (**2012**) 086; P. Giardino, K. Kannike, M. Raidal, and A. Strumia, *ibid.* 06 (**2012**) 117; D. Carmi, A. Falkowski, E. Kuflik, and T. Volansky, *ibid.* 07 (**2012**) 136; A. Djouadi and G. Moreau, arXiv:1303.6591.

[12] J. Ellis and T. You, J. High Energy Phys. 09 (**2012**) 123.

[13] J. Ellis and T. You, J. High Energy Phys. 06 (**2012**) 140.

[14] G. F. Guidice, C. Grojean, A. Pomarol, and R. Ratazzi, J. High Energy Phys. 06 (**2007**) 045.

[15] R. Grober and M. Muhlleitner, J. High Energy Phys. 06 (**2011**) 020; R. Contino, C. Grojean, M. Moretti, F. Piccinini, and R. Ratazzi, *ibid.* 05 (**2010**) 089.

[16] M. Dolan, C. Englert, and M. Spannowsky, Phys. Rev. D **87**, 055002 (2013); A. Azatov, R. Contino, and J. Galloway, J. High Energy Phys. 04 (**2012**) 127.

[17] J. R. Espinosa, C. Grojean, M. Muhlleitner, and M. Trott, J. High Energy Phys. 05 (**2012**) 097; J. High Energy Phys. 12 (**2012**) 045.

[18] CMS Collaboration, Report no. CMS-PAS-HIG-13-005, https://cds.cern.ch/record/1542387; ATLAS Collaboration, Phys. Lett. B **726**, 88 (2013).

[19] A. David, A. Denner, M. Duhrssen, M. Grazzini, C. Grojean, G. Passarino, M. Schumacher, M. Spira, G. Weiglein, and M. Zanetti, arXiv:1209.0040.

[20] F. Hubaut, in Rencontres de Moriond EW 2013, La Thuile, Italy, 2013 (to be published), http://cds.cern.ch/record/1532449/files/ATL-PHYS-SLIDE-2013-113.pdf; G.Gomez-Ceballos, in Rencontres de Moriond EW 2013, La Thuile, Italy, 2013 (to be published), https://indico.in2p3.fr/getFile.py/access?contribId=16&sessionId=6&resId=0&materialId=slides&confId=7411.

[21] A. Djouadi, Phys. Rep. **457**, 1 (2008).

[22] J. Ellis, M. K. Gaillard, and D. V. Nanopoulos, Nucl. Phys. **B106**, 292 (1976).

[23] A. Djouadi, J. Kalinowski, and M. Spira, Comput. Phys. Commun. **108**, 56 (1998).

[24] J. R. Espinosa, M. Muhlleitner, C. Grojean, and M. Trott, J. High Energy Phys. 09 (**2012**) 126; S. Kraml *et al.*, Eur. Phys. J. C **72**, 1976 (2012); A. Azatov, R. Contino, and J. Galloway, J. High Energy Phys. 04 (**2012**) 127; J. High Energy Phys. 04 (**2013**) 140.

[25] S. Dittmaier *et al.* (LHC Higgs Cross Section Working Group), arXiv:1101.0593.

[26] M. Grunewald *et al.*, CERN Report No. 2000-09-A, Part 1.

[27] E. Boos, V. Bunichev, M. Dubinin, L. Dudko, V. Edneral, V. Ilyin, A. Kryukov, V. Savrin, A. Semenov, and A. Sherstnev, Nucl. Instrum. Methods Phys. Res., Sect. A **534**, 250 (2004); A. Pukhov *et al.*, arXiv:hep-ph/9908288; see also http://theory.npi.msu.su/comphep.

[28] D. Zanzi (ATLAS Collaboration), in European Linear Collider Workshop, DESY, Hamburg, Germany, 2013 (to be published); A. Savin (CMS Collaboration), in European Linear Collider Workshop, DESY, Hamburg, Germany, 2013 (to be published).

[29] J. Ellis and T. You, J. High Energy Phys. 06 (**2013**) 103.

[30] See http://moriond.in2p3.fr/QCD/2013/MorQCD13Prog.html.